Imperial College London

DMT Group 10B

Mechatronics Outreach

Product Presentation, Analysis and Test Report

Superproject supervisor:	Richard Van Arkel
Project Supervisor:	Ferdinando Rodriguez y Baena
Project:	DMT Testing and Analysis Report
Academic Year:	2022-2023
Authors:	Saom Anisi, Alex Hayward, Matthias Jammot, Oliver Langton, Omar Sorour
Date:	7 June 2023

Department of Mechanical Engineering

Imperial College London

Version 3.5

Executive Summary

A decline in undergraduates studying engineering and entering the industry (Luke Armitage, 2020) has prompted a surge in funding and interest among academics and current leaders in the field to inspire a new generation of young engineers. A project was assigned to five Mechanical Engineering Students at Imperial College London to design, manufacture and test a device, as part of a wider superproject aimed at 11-14 year olds, tasked with showcasing different possibilities in the field of Mechatronics to inspire adoption of the technical subjects required to pursue a career in the field.

The device consists of a conveyor belt featuring obstacles that must be avoided. A pin moves orthogonally to the belt direction, with the aim of avoiding the approaching obstacles. This is done using three user modes of operation:

1. Manipulating a joystick to move a pin left or right along a continuous range of positions
2. Manipulating a joystick to move a pin to one of three discrete positions
3. Fully automated machine-vision control

This report presents an overview of the device functionality and the operation of key subassemblies and subsystems developed since the manufacturing review. It then explains two tests. The first evaluates whether the controller-perceived position of the pin changes significantly over time, leading to inaccurate positional commands by the controller. The second tests whether the speed of the movement of the pin is fast enough to properly operate the device in the 3 modes while demonstrating the benefits of electromechanical control and automation with respect to repetitive and time critical tasks. The device successfully operates in all 3 modes, meeting all PDS requirements (Anisi, Jammot, Hayward, Langton, & Sorour, 2023) including requirements for mass and size, except for being 15% slower in the second test than the PDS demanded. This result was deemed acceptable within the scope of the objectives of the project.

Literature Review

A literature review was conducted to find qualities of successful outreach programmes to identify strategies to increase effectiveness and achievability of the project goals. The efficacy of the attributes that make a successful outreach programme are not very well researched specifically for a mechatronics outreach project. However, details of engineering outreach methods appeared to be well documented, although with varying qualitative measures of effectiveness due to a diverse range of variables, methods and objectives set.

According to A.Jeffers, A.G.Safferman, S.I.Safferman (2004), after reviewing over fifty-five K-12 (education before university) engineering outreach programmes, recurring themes were “active learning through hands on experiences” and “inquiry-based learning”. This is in agreement with A.B.Anthony et al (2016) that points out that observation, as occurs with a functioning physical demonstration device, is a method of inquiry based learning that awakens curiosity. By focusing on an arcade game with a very ‘hands on’ approach, this project aims to maximise its target group’s interaction with the field of Mechatronics to inspire them to become engineers. The mechatronic concept of control is exemplified through a progression in the user’s automation for them to have an immediate understanding of the benefits of control algorithms. A study conducted by C.V.D.Carvalho et al (2018) showed a positive correlation exists between a student's enjoyment of an engineering-based game and their desire to pursue an engineering career. The user will have visual feedback of full automation performing better than they will be which, through visual acknowledgement, will likely generate inquiries as to how the control aspects of the project work and how they are beneficial.

Overview of the Superproject

This project is part of a wider superproject aimed at increasing engagement among 11-14 year old secondary school students with the aim of inspiring more individuals to opt for engineering-aligned subjects at GCSE and A level such as Mathematics and Physics. The traditional teaching of these subjects at educational institutions may have dissuaded potential engineers from pursuing a career in the field, and this approach aims to provide a more tangible and exciting experience. Six demonstration devices were set to be produced, each representing a field of Mechanical Engineering with which the Department is heavily involved with at Imperial College London. The six fields include: Mechatronics; Structural Mechanics; Fuel Cells; Lubrication, Friction and Wear; Thermofluids; Batteries.

An added layer of refinement was made where subprojects were divided amongst two suitcases. The suitcase assigned to the Mechatronics Project also contained the Structural Dynamics Device as well as the Fuel Cell Demonstrator. The project directors specified that all three projects needed to fit in the assigned suitcase, as shown in Figure 1a. The summaries of these three projects are outlined below.

Mechatronics Outreach: A device aimed to show the benefits of electromechanical control and automation for the conduction of repetitive and time critical tasks through the actuation of a collision avoidance system. The user's control is increasingly automated to illustrate this purpose.

Solid Mechanics: A device built to demonstrate projectile motion and energy transfer in the form of a high-jump-inspired demonstrator.

Fuel Cell Demo Kit: A working fuel cell demonstrating the concepts of energy production and electrochemistry using fuels such as lemon tea, apple juice and alcohol, with salt water being used as an electrolyte. Introduction of the fuel and electrolyte produces a voltage which is clearly displayed.

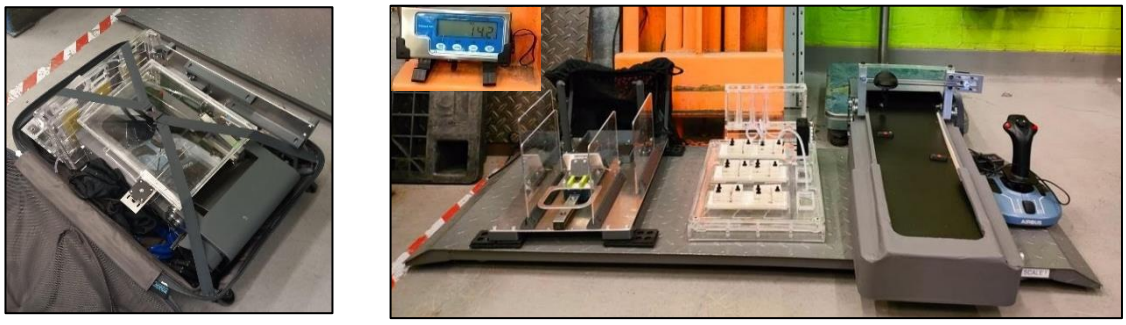

a) **b)**

Figure 1: **a)** Devices fitting into a 760x500x320mm suitcase **b)** Overview of the different subprojects

A common budget of £3000 was agreed to. Each group has roughly spent £1000 to date; however, the team requested a more powerful microprocessor for smoother machine vision and augmented reality rendering, increasing the project's budget to a total of £1200.

An emphasis was placed on creating a safe design with a total maximum mass of 23kg per suitcase. The demonstration should last 5 years with minor repairs or require easily reproducible components through processes such as small-scale additive manufacture. The total mass of the three devices was 14.2kg, with adequate room for additional accessories, as shown in Figure 1b. The total mass of the suitcase and internals amounted to 20.2kg. Interfacing between projects involved the transfer of engineering experience, technical feedback, organisation of space within the common suitcase, which required extensive communication through the manufacturing phase and its corresponding design stages. Our early completion of design and manufacturing gateways yielded the added benefit of being able to share experience with the other groups about problems encountered and solutions implemented to assist with their prototype development.

Project description

Device Overview

The Mechatronics outreach device is an arcade-like game in which the user tries to avoid approaching obstacles ('asteroids') on a conveyor belt by moving a rocket-shaped pin (hereafter referred to as just the 'pin') left and right. Following the product's theme, it has been named 'The Asteroid Belt'. The goal of the game is to avoid as many obstacles as possible to beat a set high score. The obstacle belt's speed is adjustable for greater difficulty. The setup time is 5 minutes, satisfying PDS point 12[App. A4 PDS-12].

As previously mentioned, the pin is actuated in three distinct modes to illustrate the advantages of automation and control for repetitive and time critical tasks. Mode 1 consists in the user navigating the rocket right or left by tilting the joystick. This mode allows a continuous variation in position of the rocket from side to side, requiring precision and dexterity from the user. Mode 2 is similar to Mode 1 with the difference that the pin can take one of three possible discrete positions (left, middle, right). A greater emphasis on reaction time is placed here as precision is no longer required to avoid the obstacles. The third mode is fully automated and uses a machine vision algorithm to detect obstacles and their positions, actuating a stepper motor to move the rocket autonomously. Progressing through the modes results in a lower mental load being applied on the user due to the progressive automation of tasks, leading to a greater consistency and accuracy observed over time.

The full device assembly has two principal subassemblies: the conveyor belt mechanism delivering asteroid obstacles towards the rocket, and the user-controlled rocket subassembly. A more detailed breakdown is illustrated in Figure 2b [App. A4 PDS-1,5] pertaining to purpose and ergonomics.

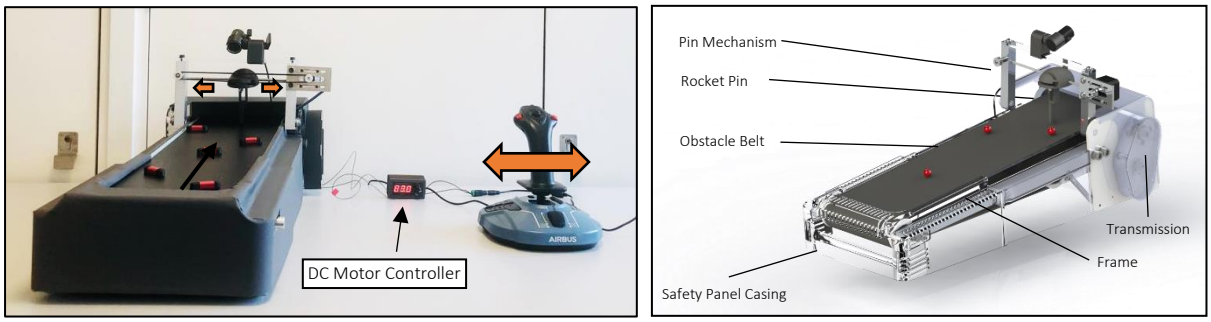

Figure 2: **a)** Picture of the general assembly **b)** Main components of the Asteroid Belt

Key features and Subassemblies

Pin Subassembly

The pin subassembly is responsible for the obstacle avoidance. The subassembly consists of two vertical aluminium struts which hold up the subassembly. These struts are placed on two steel pins that slide into the frame which allow rotation of the whole pin subassembly for stowage in the suitcase, as shown in Figure 3.

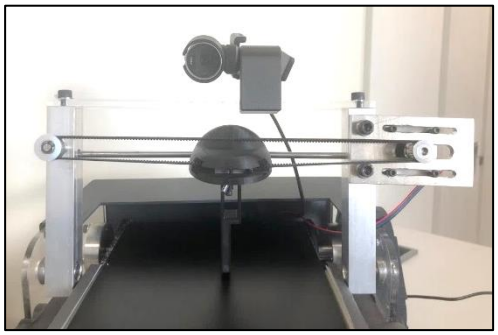

Figure 3: Picture of the Pin Subassembly

Movement of the pin is controlled by the actuation of a toothed belt wrapped around two pulleys. One pulley is secured to a stepper motor driving the pulley rotation, with the other free to rotate on an integrated bearing. The stepper motor is face-mounted on an aluminium motor plate with adjustable positioning to ensure the belt is tensioned. Spanning the two vertical struts is a steel bush shaft (h6 tolerance) on which the pin itself moves from side to side through a linear bearing. An acrylic connecting beam is

attached to the top faces of the vertical struts to secure the camera mount. Note that all bending stress is transferred to the silver steel rod itself, the acrylic beam's sole purpose being to mount the camera. The aluminium housing for the bearing is crimped to the belt via a wingnut-bolt configuration for ease of use. A 3D-printed ABS shell is fitted onto the linear bearing housing both to constrain the bearing and for the 3D-printed rocket to attach to it. [App. A4 PDS-15]

Belt and frame subassembly

The belt subassembly's purpose is to move the obstacles the pin has to avoid. The obstacles, situated in three lanes, are attached to the belt via glue dots for ease of maintenance and safety upon collision with the pin [App. A4 PDS-16] which states obstacles must be securely fastened and tested. The subassembly consists of three drums secured on aluminium 6061 shafts with a belt wrapped around them. The shafts were made of aluminium to meet the PDS requirements for mass and size. [App. A4 PDS-3] The team was aware of aluminium's susceptibility for shear failure and disintegration tendencies when interfaced with a bearing or similar fixture. However, considering the very low loading conditions and the fact that two of three shafts are fixed rather than rotating, this decision was proved necessary through extensive calculations and discussion with project supervisors.

The conveyor belt tensioning mechanism is achieved using one of the three drums. Extension of the frame activates the idler mechanism, as exemplified in Figure 4a and 4b. As the frame extends to the locking position, the belt becomes taught and forces the idler drum to lift off the tabletop. Both the weight of the idler drum and the extension of two springs provide a tensioning force on the belt downwards. This idler mechanism can adjust for belt stretch over time and general wear with a clearance of 20mm, meaning a decrease of 10mm in frame capacity is theoretically tolerable before the idler drum begins rubbing on the tabletop if the frame was to be modified.

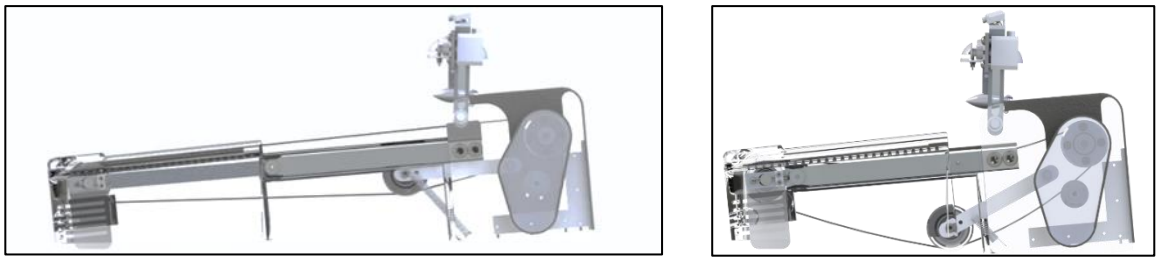

a) b)

Figure 4: **a)** Extended configuration (in-use) **b)** Shrunk configuration (suitcase)

The device's extension mechanism increases the device's length from 51cm to 72cm. [App. A4 PDS-17] Extendable light aluminium arms, consisting of an inner and outer parts, constitute the mechanism of securement, similar to that of an extendable umbrella. A compressed spring pin extends once it reaches a hole, locking the extendable arms in place, shown in Figure 5a. [App. A4 PDS-2,14] For retraction, the device is shrunk by pushing the front and rear panels towards each other, illustrated in Figure 5b. It allows for increased user excitement by having a less repetitive obstacle course. [App. A4 PDS-10]

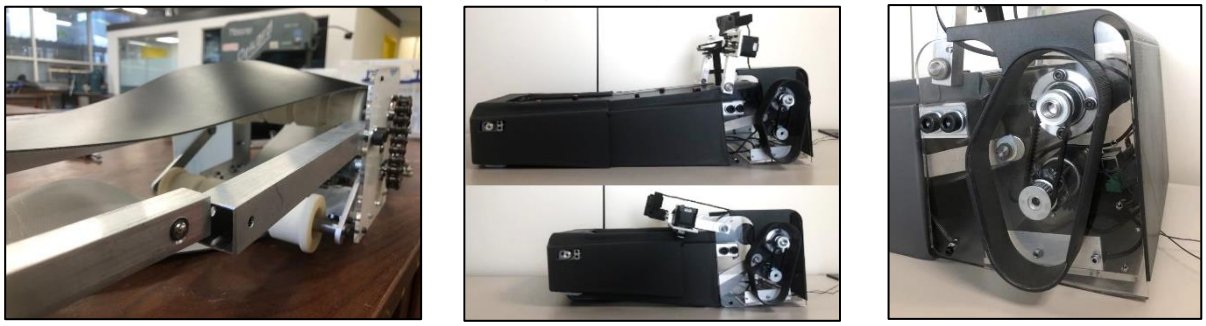

a) b) c)

Figure 5: **a)** Locking Mechanism for Frame Extension **b)** Picture of the extended / compact Asteroid Belt configuration 510x320x200mm **c)** Picture of transparent panels showcasing mechatronics system

For the belt to be rotated, a motor mounted on the frame transfers rotation to the driver shaft via a pair of pulleys and a toothed belt, illustrated in Figure 5c. Previously the rotation was transmitted to the motor via a chain and sprocket system. However, this produced excessive vibration which affected camera tracking, and was 400g heavier than the pulley and toothed belts.

To aid the educational and inspirational goals of the project and to allow the children to understand the mechanisms behind the function of the assembly, the frame incorporates clear acrylic panels to showcase internal electronics and mechanisms, depicted in Figure 5c. [App. A4 PDS-4] The device also features a transmission window for children to clearly identify the pulley system. Further to this, the device's peripheral control makes it accessible for children with disabilities who require specialised equipment for interfacing with computers. Keyboards may also be easily remapped to make the user experience more suitable and engaging for such groups. Another exciting feature of this subassembly is a mechanism adjusting shaft alignment to prevent belt derailment caused by belt drift (Appendix A1).

Safety Features

Given the device's target users are children, robust safety features were highlighted as crucial. While several safety concerns were identified and designed for (e.g. electronics), the greatest design challenge was to ensure all moving parts were contained to eliminate the risk of trapping.

The primary strategy for this was to print four 'frame cover' parts using additive manufacture in order to protect users from the moving belt and belt transmission. [App. A4 PDS-9] This manufacturing technique was selected for its precision and flexibility, required to produce the complex interlocking rail system to allow the product to be collapsible and have soft filleted edges. Figures 6a and 6b show how these panels were assembled. The rear panel is integrated with a clear window to showcase the transmission safely, with the side panels featuring a complementary rail to the front panel's carriage profile, shown in Figure 6c. This component is needed to interface with roughly 8 stationary components and two rotary, whilst leaving adequate clearance for belt-mounted obstacles. The light prints were wrapped in smooth space grey film for colour continuity. [App. A4 PDS-6]

a) **b)** **c)**

Figure 6: **a)** 3D printed protective transmission cover **b)** 3D printed protective frame cover **c)** Smooth space grey film providing colour continuity

Hardware-Software Development and Integration

To supply power to the electronic components, AC/DC converters were used to save mass and space over an equivalently suitable power supply unit. This eliminates the battery capacity constraint. [App. A4 PDS-11] All the electronic systems are controlled centrally from a Raspberry Pi 4 (except for the DC motor) that runs a program on boot to automatically start the game. [App. A4 PDS-19] This is shown in Figure 7a.

The computer vision-aided third mode detects obstacles and their positions using a 720p resolution camera. [App. A4 PDS-18] To engage an entire classroom as well as the individual user, the machine vision detection is visible in the device output. [App. A4 PDS-7,10] Image segmentation and obstacle

detection is presented in an engaging way, with differences between unaltered camera feed and machine vision output clearly visible. In Figure 7b, the green lane indicates the pin's next position, red the lane blocked by the obstacle, and the numbers the order of priority. The camera mount is manufactured from carbon reinforced filament, ideal for this application due to the gripping the camera requires, supplied by the material's stiffness. The mount includes an adjustable arm, with the square mounting bore providing a tight fit to the supporting bar with 0.15mm clearance, allowing the mount to be adjusted axially, as shown in Figure 7c. The result is a robust camera mount allowing computer vision input.

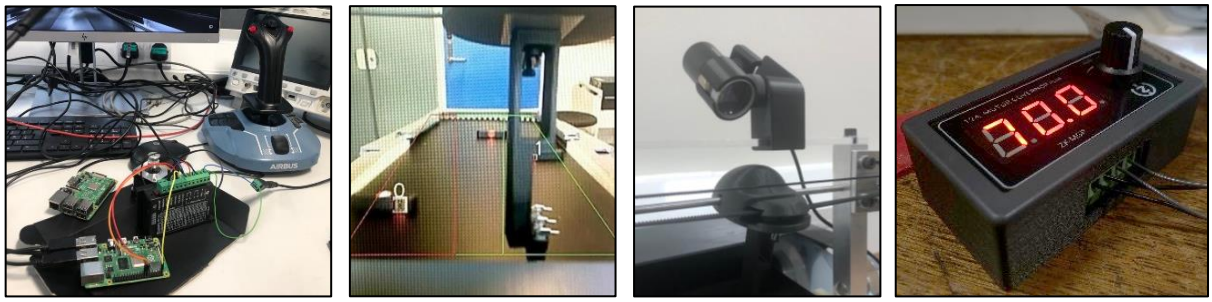

a) b) c) d)

Figure 7: **a)** Electronic components (Motor Driver, Stepper Motor & Raspberry Pi 4) **b)** Computer Vision Obstacle Detection **c)** Camera Mount (Carbon Filament) **d)** 12V DC Motor Controller

The conveyor belt is powered by a brushed DC motor, manually controlled by a 12V DC motor controller, depicted in Figure 7d. This converts a DC connection to a PWM wave with adjustable frequency, controlling the duty cycle supplied to the motor and therefore the belt speed. This features an integrated switch/rotary controller with percentage readout. This is housed externally, allowing greater accessibility for interaction instead of a side panel mounted solution which may not be visible.

In its entirety, the code spans roughly a thousand lines of code with low latency, with around five thousand lines of test code having been written in total. The code shows the user interface and highlights free paths, providing a visual representation of the algorithm instructions to the stepper motor. The joystick and limit switch collision avoidance system integrate seamlessly with the main hardware via a USB interface and board pin input/output. Multithreading is employed for simultaneous image processing/segmentation and motor control, as well as playing our theme tune! [App. A4 PDS-8]

Budget Overview

During the initial project briefing, £1000 was allocated to the development of each device in the superproject. A full breakdown of the budget is available in Appendix A2. Hereafter follows a summary of the most important takeaways. An additional £200 was granted to buy a more powerful microprocessor (8GB RAM, Raspberry Pi 4) instead of the original 1GB RAM Raspberry Pi 4 originally purchased. This was due to a computational requirement of rendering augmented reality overlays over the camera feed and overall smooth running of the computer vision system, something the lower specification microcontroller was struggling to accomplish. Moreover, a faster stepper motor speed and latency was observed during software testing on the new hardware. The joystick was suggested at the Manufacturing Gateway and was absorbed by the initial budget at a cost of £51. This resulted in an enthusiastic sentiment surrounding the device, with peers asking to have a go based on what they could see.

Materials for in-house manufacturing consisted of a very minor proportion of budget – less than 10% of overall costs. Electronics amounted to 40%, the rest being spent on parts that were manufactured externally or on directly purchased components.

Test report 1

The first test concerns motor accuracy. The aim of this test is to establish whether the deviation of the true rocket pin position relative to the demanded position from the control algorithm over time is acceptable and within range of the product design specification. This is especially pertinent as the pin actuation is open-loop-controlled and therefore does not have feedback to correct positional errors. Its position must be reasonably accurate for an extended period of time before recalibration. The PDS-specified maximum drift rate is a 95% confidence that the pin drift will not exceed 5mm after 10 minutes of play. The reasoning behind this requirement is to ensure the pin drift does not become too large to either be noticed by a user or to significantly affect gameplay before re-calibration is required.

Test Description

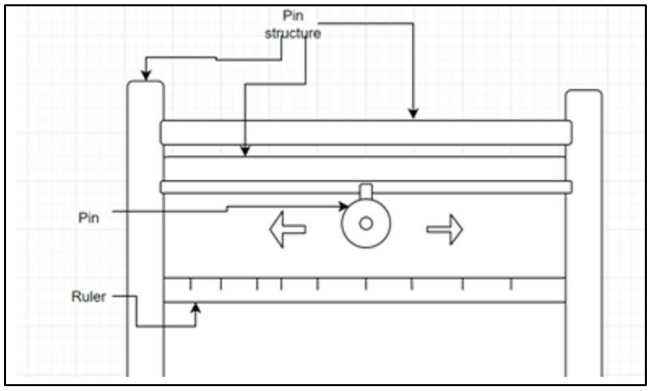

Figure 8: Model of the Test 1 set-up

The underlying principle behind conducting this test was to simulate gameplay by moving the pin back and forth to random positions as experienced in Mode 2 under joystick control. Following random movement for 180 seconds the pin halts for its position to be recorded. This is repeated 20 times for a total run time of one hour. The setup is illustrated in Figure 8. A ruler graduated in millimetres is fixed across the pin struts, resting on the frame panels for horizontal alignment with no further modifications to the pin structure. Care was taken to align the ruler horizontally to prevent error in the measured distances from misalignment. Each 3-minute run started and ended with the pin in the controller-perceived centre position. The centre position was then recorded against the fixed scale with a set square to reduce parallax error after each run. A 30 second time interval between runs was introduced in the testing algorithm to allow for measurements to be taken. A camera was also set up on a free-standing tripod, isolated from the device, during testing. This was done to limit human error such as lapses in concentration and eliminate the possibility of failing to take a reading. Care was taken to align the camera level with the ruler graduations with a spirit level used to ensure horizontal alignment. The recording provided additional data points for additional comparisons with measured values and allowed critical analysis of error sources which provided general information about pin assembly behaviour. The appropriate resolution camera was sourced with adequate resolution to clearly distinguish the ruler scale at a 1m distance. Use of a tripod was crucial to ensure stability and positional consistency with respect to camera angle throughout the experimental period.

The three positions are programmed in terms of steps within the computer vision algorithm. This means that the theoretical position of the pin at any one time is known, making the test valid for all three user modes of operation as these rely on the controller's accurate record of the pin's true position to function. For instance, to stop the pin crashing into the pin mechanism structure or to instigate switching tracks. For modes 2 and 3, the movement in-between tracks occurs at the same speed than that of the test, indicating that this variable is correctly controlled. For mode 1, the pin's movement speed is slower than modes 2 and 3 due to real-time continuous monitoring of joystick input, so if pin drift is low due to the motor skipping steps at higher speeds, it is very unlikely to occur at lower speeds.

Predicted performance

A precedent exists for the use of stepper motors in similar applications. They are common in 3D printers, which heavily rely upon rapid and precise movement feedback (Imperial College London Mechanical Engineeinrg Department, 2022). The stepper motors typically operate without feedback (open-loop control) and may thus reliably position themselves quickly without skipping steps. A similar performance without drift is hence expected for this project.

A pull-out curve gives the maximum possible torque a stepper motor can bear for a given pulse rate. The curve for the motor of the pin assembly is given by the light blue line in Figure 9a. More important to the pin drift, however, is the pull-in curve. While the pull-out curve gives the maximum steady-state output speed for a motor, this does not entail that the motor can accelerate from zero to that speed instantaneously. Instead, to achieve such acceleration it needs to aim for an intermediate speed given by the pull-in curve as illustrated in Figure 9b. After attaining that speed, it can then be accelerated to the speed given by the pull-out curve. Cases for which this procedure is not respected may lead the stepper motor to skip steps, causing pin drift. While the pull-out curve was provided by the manufacturer of the stepper motor, the pull-in curve was not. The PDS demands high pin acceleration from a stopped position (especially in mode 2 and mode 3), and it is desirable to accelerate the stepper motor as fast as possible to optimise latency, but that must be balanced against the feasibility of doing so, given the pull-in torque and the loading conditions. Thus, testing must determine whether the pulse delivery schemes would give the desired performance, and to adjust such schemes if necessary.

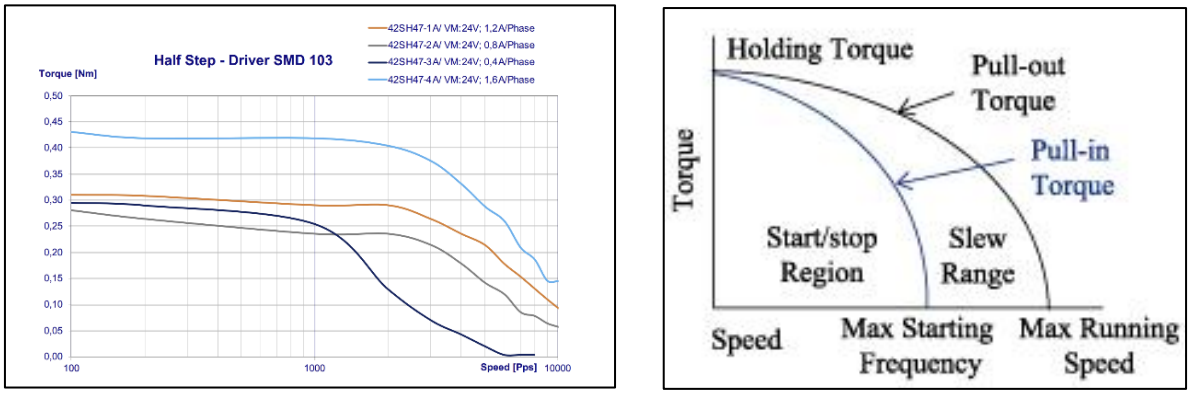

a) b)

Figure 9: **a)** Stepper motor pull-out torque graph (Delta Line) **b)** Graph illustrating pull-in torque (MinebeaMitsumi, n.d.)

Measured Performance

Initial testing of the pin showed significant, readily observable deviations from the desired position, which was in disagreement with the PDS. The three tracks the pin could move into (for modes 2 and 3) were evenly distributed on the rail, but for certain measurements the pin clearly moved a small fraction of the distance between them, and over multiple commands to change positions, would quickly collide with the sides of the pin assembly. The initial algorithm for the control of the stepper motor acceleration did not take pull-in torque into consideration. It assumed the stepper motor could reach the desired speed instantaneously and the pulse rate did not introduce any ramping – with a constant rate starting from zero angular velocity. After extensive experimentation, subsequent adjustments, and iteration, a trapezoidal velocity scheme (constant acceleration to the maximum velocity, held for a time, then constant deceleration) was implemented, which gave far better visual results. To verify the better visual results translated to meeting the PDS, the test outlined in the description above was conducted. Table 1 presents the results of this test.

Table 1: Results of the Pin Drift Test

Time elapsed (mins)	Ruler value (cm)	Changed reference point		
		Centre (cm)	Left side (cm)	Right side (cm)
0	10.6	12.8	8.0	17.8
3	10.6	12.8		
6	10.6	12.8		
9	10.6	12.8	7.9	17.7
12	10.6	12.8		
15	10.6	12.9		
18	10.7	12.9	7.9	17.7
21	10.7	12.8		
24	10.6	12.8		
27	10.6	12.8	7.9	17.7
30	10.5	12.8		
33	10.7	12.8		
36	10.6	12.8	7.9	17.7
39	10.7	12.8		
42	10.7	12.8		
45	10.6	12.8	7.9	17.7
48	10.7	12.8		
51	10.7	12.8		
54	10.6	12.8	7.9	17.7
57	10.7	12.8		
60	10.6	12.8		

In Table 1, the “ruler value” column indicates the values of the centre track measured against the fixed ruler by eye in the lab. The “centre”, “left side”, and “right side” columns respectively show the measurements taken for the corresponding three track positions from the recorded video. The drift value for the tracks in each of these columns is the deviation from the starting position given at time = 0 minutes. Figure 10 shows a graph of the pin drift from the starting position for the “centre” column over time. Considering the error bars, the pin drift is null.

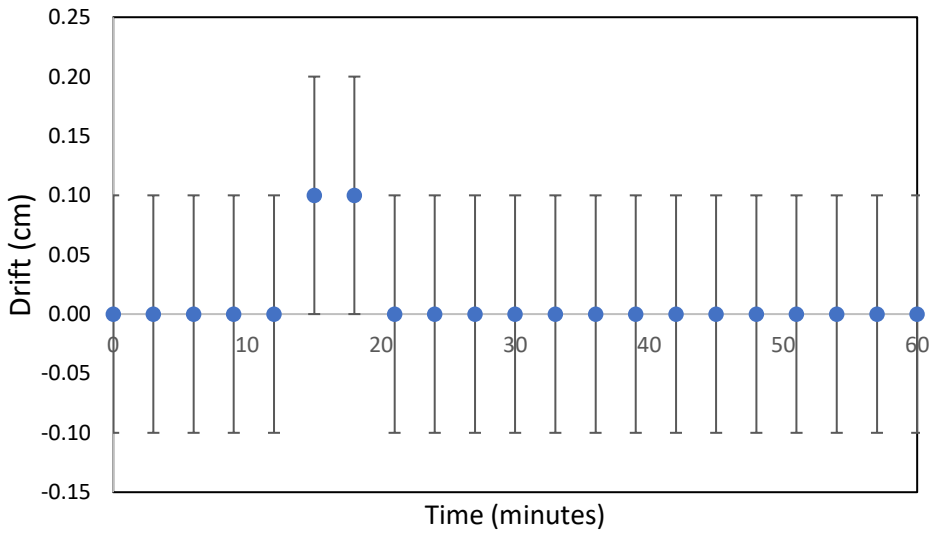

Figure 10: Drift Position from Centre Position over time

As an additional check beyond just measuring the drift in the centre position, the video footage was analysed to verify there was no drift in the right and left track positions. The method slightly differed to the previous one. Firstly, fewer measurements were taken due to the centre measurement's reliability suggesting the device's proper functioning for the left and right tracks. Secondly, the video recorded the first occurrence of the corresponding track position movement during the run specified, since the algorithm was not programmed to pause specifically at the end of 3 minutes for each run on the left and right tracks, only on the centre track.

Figure 11 shows a photo of the test set-up with the reference positions used for the measurements. The reference points for the columns in Table 1 were indeed different. The reference point for the "ruler value" column was the right flange of the wing nut. The reference point for the three other columns was the right side of the pin shell. Note that measurements were taken very carefully for the video data by using a digital ruler fixed to the vertical position. This was done to give the taped ruler's reading across the pin subassembly. The reference point was changed since in the video the angle of the camera made it difficult to see the ruler markings with the original reference point. Additionally, the presence of play in the loosening wingnut made a change in reference point necessary to acquire more reliable data. Moreover, measurements for the right and left tracks were taken less frequently, since these particular measurements consisted in sanity checks. The inconsistency in pin drift presence from the centre position strongly suggested there would be no pin drift for the other track positions, so fewer data was needed from these side tracks to infer they had no pin drift.

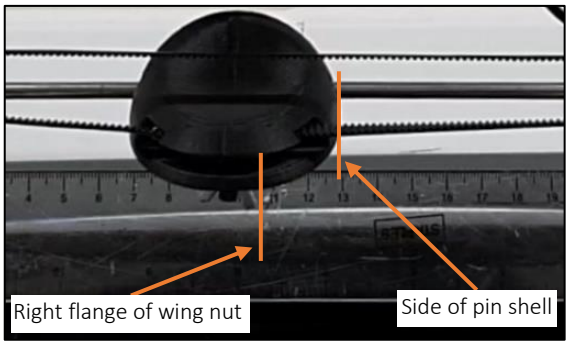

Figure 11: Pin drift measurement reference

Discussion and Conclusions

As seen from the results of the above test, the maximum error from the desired pin position is 0.1cm. This falls within the error of the measurement equipment, given the ruler has a ±0.5mm error and the true error is double this because subtraction of ruler measurements is used to calculate pin drift. It may also be observed that the pin drift does not vary significantly with time as even after 60 minutes the pin was able to return to its equilibrium position. This means that very few steps (if any) are missed which implies that the pulse delivery scheme for this stepper motor is sufficient for pin drift not to be an issue.

Potential sources of error for this experiment may have been both lens distortion from the camera and horizontal misalignment from the ruler. However, such sources of errors are negligible and inconsequential since the ruler was used to measure a small deviation from a starting position. Unless the ruler's misalignment caused the formation of a large angle, the effective distance between the pin's starting position and the measured value on the ruler is insignificant. As for the camera lens distortion, since the effective distances measured were localised to a very small portion of the frames of the video taken, this minimised the effect of lens distortion.

Test report 2

The second test for the device evaluates the same subassembly as the first. The test measured the mechanical latency in the movement of the pin between the three tracks during Mode 2 & 3. Specifically, the target figure defined in the PDS was a delay between the pin starting and finishing a positional movement from one track to an adjacent track in 0.2 seconds (justification in Appendix A3A). A second test on the pin subassembly was prioritised over testing the belt subassembly because it tests a feature important for user experience. For example, a change from Mode 1 to Mode 2 represents a significant improvement in the performance of a task through the use of active constraint systems. Most 11-14 year olds are likely to have played a game functioning on identical principles before, allowing the connection from a game they are familiar with, to the outreach device. It is important the game meets their expectations for them to be excited about the power of automation. If there is too high a lag, it is unlikely they will fully enjoy and appreciate the game. (further justification in Appendix A3B).

Test Description

In this test an algorithm was written to drive the pin to follow a series of position sequences as quickly as possible, with a pause between each sequence, as detailed in Table 3. For this experiment, there was no need to add any material or equipment to the subassembly. A phone camera was used to track the pin's position over time. The camera was held by hand since precise distances were deemed unimportant for this test given that it had already been tested in the pin drift test. Unlike the previous test, the algorithm moved onto the next position as soon as it had judged itself to have properly reached the previous one. What was indirectly measured was the time to completion of the position sequence, which was done by counting the number of frames between the pin starting to move, and the pin finishing the sequence, then dividing by the video frame rate. This was repeated three times for consistency and to improve the reliability of the results.

Predicted Performance

Latency requirements can be met for a range of different pin acceleration and maximum speed values, but there are minimums that must be exceeded. The graph in Figure 12 shows a range of possible velocity schemes over time that involve symmetrical and constant acceleration and deceleration, but that all cover a distance of 10cm (approximate distance between tracks) in a time of 0.2 seconds. Note that the red line indicates the minimum possible acceleration needed to meet the requirements but simultaneously requires the highest maximum speed. This translates to a minimum 10m/s^2 acceleration requirement and 1m/s speed requirement from the motor. The blue line indicates the minimum possible maximum speed required (assuming infinite acceleration). The green line indicates a trapezoidal velocity scheme, which was implemented in the code following testing.

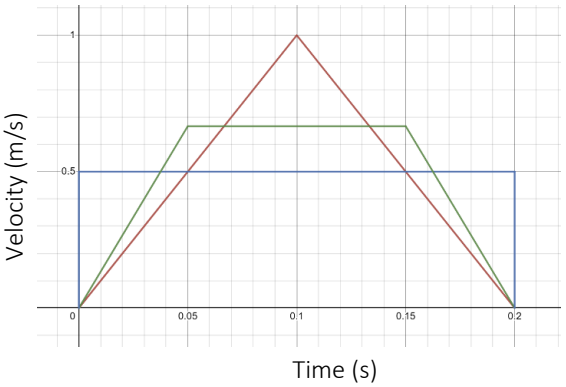

Figure 12: Pin movement velocity schemes

The specification for the pin stepper motor was given in Figure 9a, as indicated by the light blue line. It shows a maximum pulse-per-second of 10000 for the stepper motor, which has a step angle of 1.8°, which with a timing belt pulley of radius 9mm gives a maximum speed of 2.83m/s for the pin. This exceeds by far the maximum possible speed of 1m/s in Figure 12 for any velocity scheme with constant

acceleration. This indicates that the motor should be able to meet the maximum speed required for any of the velocity schemes in Figure 12. Yet, this means latency becomes dependent on torque needed to accelerate the pin to overcome the frictional forces. If the frictional forces are too high, the pin will not be able to accelerate to its maximum speed since the torque demand would be too high. The torque load will also depend on the required pin acceleration.

A model of the system allows the torque to be determined for a given velocity scheme. The model for this system is exemplified in Figure 13 (See a more detailed version in Appendix A3C). The pin subassembly may be simplified by combining the masses of the linear bearing, rocket, shell, pin holder, and by combining the moments of inertia of the pulleys and the motor into as illustrated below:

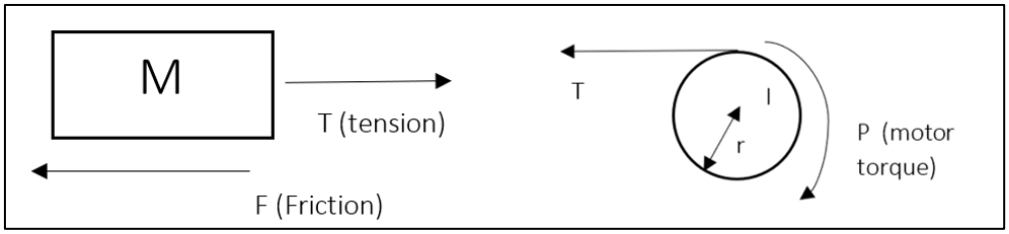

Figure 13: Simplified model of pin subassembly

A full derivation of the equations governing the acceleration of the pin involves using Newton's second law and a model for the bearing friction is fully presented in the Appendix A3C. A key assumption is that friction does not vary with speed. The result of this derivation is:

$$a = \frac{\frac{P}{r}}{\frac{M}{1-\frac{2\mu D_1}{L_1}+\frac{I}{r^2}}} \quad (1)$$

where each parameter is described in Table 2.

Table 2: Parameters of Equation 1

Parameter	Value	Unit	Description
M	0.1	Kg	Combined sum of linear bearing, rocket, shell, pin holder, fasteners to give effective mass from moving pin
I	7.04×10^{-6}	Kgm^2	Combined sum of pulley and motor moment of inertia
D_1	0.03	m	Distance of toothed belt from linear bearing centreline
L_1	0.022	m	Length of linear bearing
P	Variable	Nm	Maximum torque provided by motor at maximum speed of velocity scheme
μ	0.003-0.01		Typical value for a linear bearing of friction coefficient (Schroeder, 2017)
r	0.009	m	Pulley radius

As a proof of concept that the PDS can be fulfilled by using at least one velocity scheme, theoretical calculations for an arbitrary scheme are performed. The triangular (red) scheme was chosen for

simplicity. This means a necessary acceleration of $a = 10$ m/s^2 must be possible for the torque given the pin's maximum speed of 1 m/s which was $P = 0.35$ Nm.

In terms of the results of this model, for $\mu = 0.003, a = 207.6$ m/s^2. This far exceeds the necessary $a = 10$ m/s^2. Indeed, the limiting μ value is actually $\mu = 0.66$ for the necessary acceleration value, which far exceeds what a linear bearing should ever have. These calculations predict that, so long as the stepper motor is able to accelerate at the minimum necessary rate of $a = 10$ m/s^2 from the perspective of pull-in torque, the PDS requirements can be satisfied. To be precise, the minimum necessary pull-in torque value is $P = 0.017$ Nm (value obtained from rearrangement of Equation 1) for $\mu = 0.003$, for $\mu = 0.3$ (almost impossibly high for a linear bearing) the pull-in torque is still $P = 0.024$ Nm. Either way, the pull-in torque would have to be over 10 times lower than the pull-out torque at the maximum speed, which is unlikely.

Note, the above calculations are a proof-of-concept to determine whether the motor should be able to reach the latency demanded by the PDS given the motor's technical specification and a simplified model of the load conditions. They do not predict the mechanical latency values (in terms of time) themselves.

Measured Performance

Table 3 presents the results of the experiment. Note that three repeats were taken to generate increased reliable results. The "average time elapsed" column was calculated by dividing the average number of frames by the frame rate (30 Hz). The following column "Positional changes in sequence" counts the number of times the pin changed track in accordance with the PDS definition. For example, if the pin is commanded to do 1,3 it first has to move first track 1 to track 2, then to track 3. The final column is what is being checked against the PDS.

Table 3: Test 2 Results

Run number	Commanded position sequence	Number of frames to completion			Average Time Elapsed (s)	Positional changes in sequence	Average time between positions (s)
		Trial 1	Trial 2	Trial 3			
1	1, 2	7	7	7	0.23	1	0.23
2	3, 2	7	8	7	0.24	1	0.24
3	1, 3	14	14	13	0.46	2	0.23
4	3, 1	14	14	14	0.47	2	0.23
5	1, 2, 3, 2, 1	27	27	28	0.91	4	0.23
6	1, 3, 1, 3, 1	52	52	52	1.73	8	0.22
7	1, 3, 2, 3, 1, 2, 1, 3, 1	73	73	74	2.44	12	0.20

Discussion and Conclusions

The theoretical calculations concluded it should be possible to comfortably meet the PDS. However, the average value of the time to cross adjacent positions was 0.23s, a highly reliable result since it is averaged across 90 total repeats of positional changes with error ±0.012s (Appendix A3D). This exceeds the target by 15%. These latency timings came from a stepper motor that was thoroughly tuned to maximise speed while avoiding the stepper motor skipping steps. This number was relatively consistent

for whatever length of positional sequence was used and for whichever direction the pin was moving. The 6th run had a slightly reduced average time between positions, but it is not outside of error. It is difficult to explain the final value being significantly lower than the rest and outside error. From the video, it appears acceleration between positions is actually faster, despite often needing to reverse direction. However, the frame count for each image is not sufficiently high to offer conclusive results. Regardless, although this phenomenon is not explained, the fact that the pin may move faster for long position sequences is a positive from the perspective of the PDS.

There are a number of potential explanations to why the system does not achieve a latency that should theoretically be possible. During assembly the linear bearing might have been slightly damaged or the casing distorted, thereby increasing the friction coefficient or creating other complications. A manufacturing defect in the stepper motor, linear bearing, or rod could also be responsible for this result. The lack of sufficient technical specifications for each of the parts reduced their accuracy. There was no pull-in torque specified for the stepper motor, so it is not known whether the pull-in torque is very low relative to the pull-out torque. There seems to be a low probability given the allowable pull-in torque was less than 10% of the motor pull-out torque at the necessary maximum speed assuming the system had a coefficient of friction typical for a linear bearing ($\mu = 0.003$). Additionally, the attempt at optimisation of the pin movement speed might not match close enough its true possible optimum. Air resistance was not accounted for in the model, but the speeds are so low that this assumption of their negligibility is very sensible. It is likely that no single one of the factors explored above is responsible for the diminished performance relative to what should have easily been possible, but rather a combination of them. Although the PDS required a value of 0.2 seconds, in terms of the justification for setting that value of 0.2 in the first place (see Appendix A3A), being over by 15% does not significantly detract from the goals of that justification when it comes to creating a smoother user experience while playing the game (the difference is only 0.03 seconds after all).

The experiment did not test the PDS value of highest priority. Instead of timing the delay between an initial movement of the pin and a finishing movement, perhaps a more meaningful figure to use would be to time the delay between the initiation of a command to move the pin and a completed response. For mode 2 this initiation comes in the form of the joystick input, for mode 3 this comes from the camera input. The test ignored all form of lag from the input and processing stages. Such input is challenging to measure properly. For mode 3, it was possible to verify this for what is likely to be the most significant delay in such stages: the delay from the machine vision algorithm processing. It was not significant only 0.03 seconds. For mode 2, one can attempt a similar method of using timing in code, but it ultimately misses out the time delay from the input to the processor.

Conclusions and Recommendations for further work

The project's outcome may be deemed a success when evaluating the prototype's strong performance. The prototype achieved all its main aims set out in the product design specification as evidenced throughout this report and covered multiple interdisciplinary fields which provided team members with professional development and technical versatility. A minimum viable product was ready to receive feedback on the 17th February 2023. This allowed for greater time to refine features, with three distinct engineering versions of the prototype being developed as a result of direct feedback and investigation.

Despite positive feedback, some flaws were identified. The rear frame panel does not sit square on the acrylic frame, possibly due to warping of the ABS print. Printing the panels in the same colour would have been ideal to avoid such post-processing. Furthermore, by preventing internal component intersection the extension mechanism could have achieved the same fully deployed length while achieving a collapsed form 5cm smaller than was achieved. The geometry of the conveyor belt motor face-mounted holes made its positioning difficult. Selecting a different motor would have saved extensive frame panel prototyping and testing due to the thin amounts of material being left between mounting holes and bores. Clear additive filament safety panels would improve the project's illustrative purposes. However, budget constraints eliminated this option.

Due to a shortage of microprocessors, an inferior device was selected. A more performant microprocessor and a faster stepper motor would improve user experience. Also, reduced ventilation was an issue during the long test runs of the DC motor. Although overheating and loss of power rarely occurred, active cooling and increased voltage supply could reduce this risk. Besides this, more time allocation to the fine tuning of the machine vision algorithm will ensure more consistent and accurate results by reducing misdetection. Moving the camera mounting to the rear of the device behind the moving pin increases the clarity of the markers on the obstacles, also improving the accuracy in results.

Effect of Strikes on Project Progress

The quantities to be manufactured were sourced from the Bill of Materials, the number of striking days were recorded and checked against a daily manufacturing phase log, the estimated manufacturing time (minutes) of each part was sourced from Manufacturing Gateway manufacturing instructions devised.

Project resilience has been a high priority in the wake of workshop strikes and as such, extensive plans were made to mitigate this. The plan presented at the Manufacturing Review integrated four contingency days over a nine-day period with three team members available per day for maximum efficiency, with tasks assigned based on competency. To investigate the effect of the workshop strikes on the manufacturing phase of the device, spanning from the 20th January to the 6th February 2023, a score was calculated through the product of four key metrics. These consisted of the number of strike days present between the planned start date of a component and actual delivery date; the quantities required to be manufacture and the percentage of anticipated time (in minutes) of the total anticipated time to manufacture all components.

The majority of components were unaffected by the strikes due to a nullifying factor of 0 strike days between planned start and actual delivery date. In total, five critical components were directly affected by the strikes, which included the Driver Shaft (51.8), Driven Shaft (21.4), Pin Holder (18.7), Driven Pulley Vertical Strut (13.8) and the Belt Idler Shaft (12.1). The highest score components were the most affected by the strikes and featured the highest complexity, the majority were high tolerance shafts. The number of 4 strike days applied to both the driver shaft and driven shafts which reiterates the importance of feeder chain buffers in project management.

References

Andrew T.Jeffers, Angela G.Safferman, Steven I.Safferman (2004) 'Understanding K-12 Engineering Outreach P*rograms*' American Society of Civil Engineers

Anika B.Anthony,Howard Greene, Paul E.Post, Andrew Parkhurst, Xi Zhan 2016, '*Preparing university students to lead K-12 engineering outreach programmes: a design experiment*' European Journal of Engineering Education ,Vol. 41, Issue 6, pp.623-637

Carlos Vaz De Carvalhp , Manuel Caeiro-Rodri´guez, Marti´n Llamas Nistal, Melani Hromin, Andrea Bianchi, Olivier Heidmann, Hariklia Tsalapatas, Alper Metin (2018) *'Using Video Games to Promote Engineering Careers' International Journal of Engineering Education, Vol 34, Issue 2(A), pp.388-399*

Anisi, Jammot, Hayward, Langton, & Sorour. (2023). *Product Design Specification.* Imperial College London: Unpublished.

Delta Line. (n.d.). *42SH47-4A.* Retrieved from Delta Line: https://en.delta-line.com/a.pag/42sh47-4a-pzk2855kzczk209.html

Gameloft. (2022). *Minion Rush*. Available at: https://minionrush.com/ (Accessed June 2023)

Imperial College London Mechanical Engineeinrg Department. (2022). *Chapter 3 Electric Actuators.* London.

Luke Armitage, M. B. (2020). *Engineering UK 2020 Educational pathways into engineering.* Available at: https://www.engineeringuk.com/media/196594/engineering-uk-report-2020.pdf

(Accessed: June 2022)

MinebeaMitsumi. (n.d.). *Hybrid stepping motors*. MinebeaMitsumi Product Site: https://product.minebeamitsumi.com/en/technology/rotary/hybridmotor_cat-3_004.html

(Accessed: June 2022)

Schroeder, J. R. (2017, September 30). *Linear Bearings: Understanding the 2:1 Ratio and How to Overcome the Stick-Slip Phenomenon*. Machine Design. https://www.machinedesign.com/mechanical-motion-systems/article/21836017/linear-bearings-understanding-the-21-ratio-and-how-to-overcome-the-stickslip-phenomenon (Accessed: June 2022)

Appendices

A1. Shaft Alignment Mechanism

The frame also features a mechanism to adjust the shaft alignment, greatly reducing the risk of derailment of the belt due to belt drift. This consists of an M5 bolt passing through the fixed driven shaft, with a nut placed before and after the hole in the shaft, illustrated in Figure 14. This allows sub-millimetre scale adjustment to ensure the driver and driven shaft are parallel. It was found that allowing some movement of the driven shaft was optimal so the belt could self-align as opposed to being completely rigid as was the case for both ends of the driver shaft. For clarity, to increase the bias according to Figure 15, the left nut is loosened, right nut is tightened, increasing the toe/bias of the driven shaft with respect to the driver. The other side of the shaft remains fixed to the inner arm of the extension mechanism. The inner arm on the side of the adjuster features a slot instead of a threaded hole as per its counterpart.

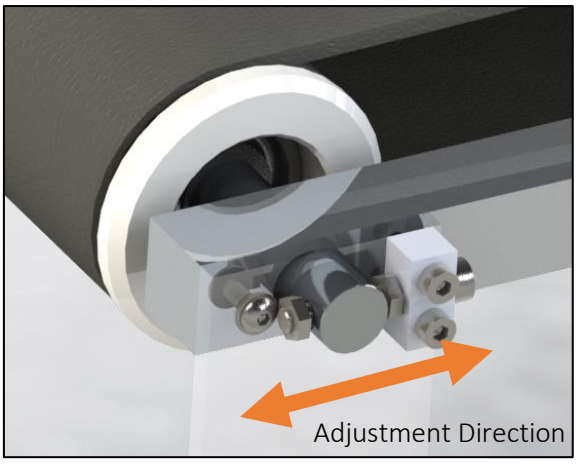

Figure 14: Zoom Shaft Alignment Mechanism

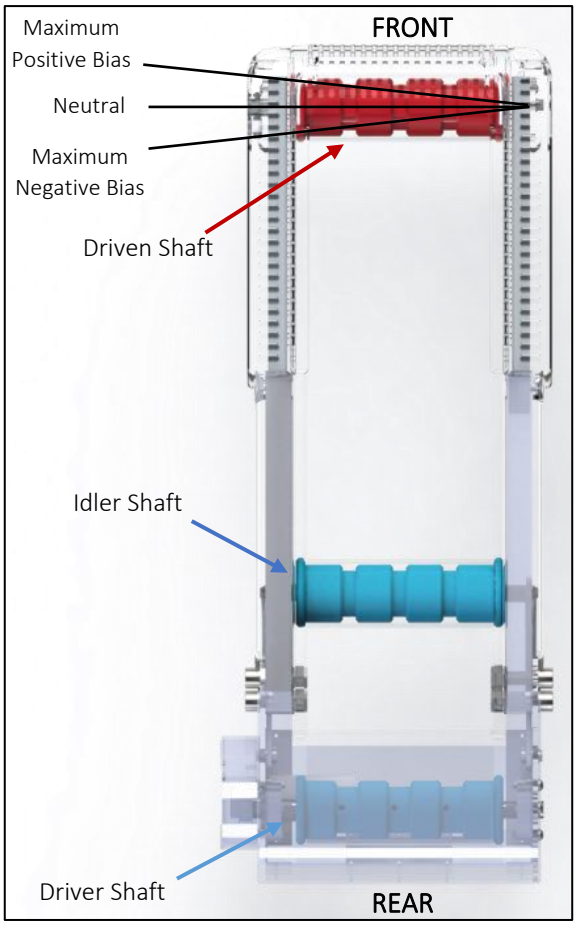

Figure 15: Bottom View Shaft Alignment

A2. Budget breakdown

Table 4: Detailed Budget Breakdown

Unit	Amount (£)
RS Purchase Order	179.59
Xometry	135.00
Pulleys and Controller	30.00
Belt	83.21
Spring pins	15.97
ME Stores	86.56
Aluminium Sq Section	19.10
Motors and controller	88.86
Enclosures	150.00
new Pi	170.00
SD card	8.00
New Drive (belt pulley drive)	27.06
Joystick	51.94
Rocker Switches	7.21
Camera Pi	6.00
Power Supply	31.80
Rpi	69.00
Total:	**1159.30**

Table 4 presents the detailed breakdown of the project's budget. The total sum spent amounts to £1159.30.

A3. Test report 2

A3A. Justification for mechanical delay of 0.2 seconds

The figure of 0.2 seconds was determined from a source of the inspiration behind the device itself. A screen recording of the play of a mobile game with gameplay identical to mode 2 (i.e. three tracks, obstacles, moving between them) called “Minion Rush” (Gameloft, 2022) was taken. The delay for the movement between tracks was consistently 5 frames for a refresh rate of 30Hz for the screen recording. This translated to 0.167 seconds time delay, and this was rounded up to 0.2 to give some leeway for the fact that exact precision was not required to give a similar experience for the mechanical device. Note that 0.2 seconds was specified for movement between adjacent tracks, so does not apply for a movement command from 1 to 3 within 0.2 seconds. This is firstly because in the “minion rush” game (and similar games) it is not possible to move directly from track 1 to 3, one must cross first to track 2 and then to 3. There is thus a game play precedent in having such a delay between extreme track positions. Furthermore, the obstacle course can be designed so that no more than one movement along the track is necessary between lines of obstacles if lag between extreme positions on the belt becomes a problem.

A3B. Justification for conducting a second test on the pin subassembly

The primary alternative test that would have been conducted for the belt assembly would be to test the belt speed. However, the exact speed at which the obstacles pass the rocket pin does not actually matter – what is most important is that there is a significant range of speeds. Beyond that, if that range of speeds is on average fast or slow, the separation of obstacles on the belt can be modified to suit the timing gap with which the next obstacle passes the pin subassembly specified in the PDS of being minimum 0.4 seconds at the belt maximum speed.

A3C. Derivation of the acceleration formula for the pin

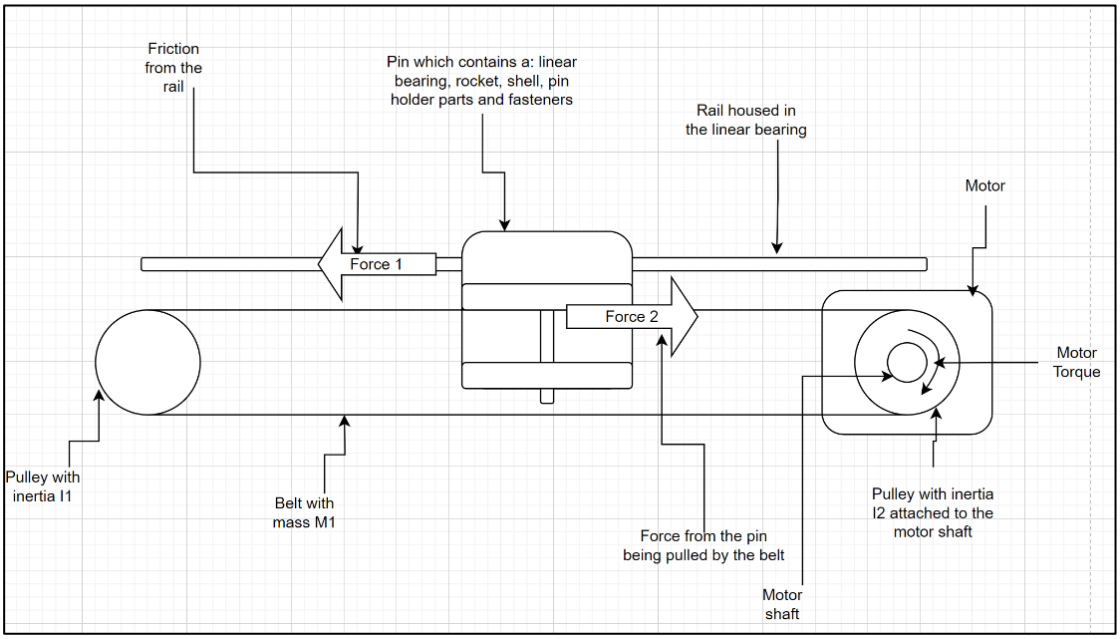

Figure 16: Pin subassembly schematic

Figure 16 aids with the visualisation of the forces and masses acting on the pin subassembly that are relevant to the pin movement. All the bodies and forces can be simplified into the free body diagram in the test report 2 section in the main body of the report.

Applying Newton's second law to each of these masses separately:

$$T = Ma + F \tag{2}$$

$$T = \frac{P}{r} - \frac{Ia}{r^2} \tag{3}$$

Let us assume that the frictional forces from the linear bearing do not vary significantly with speed. This means the maximum torque load on the motor occurs while the pin is accelerating rather than at a constant speed due to the changes in inertia of the timing belt pulleys and the pin itself (according to equation 2). The torque is constant while accelerating at all velocities because friction and acceleration are constant with speed. The pull-out torque monotonically decreases as speed increases. Therefore, the maximum torque load the motor can bear for a particular velocity scheme is given at the maximum velocity of that scheme.

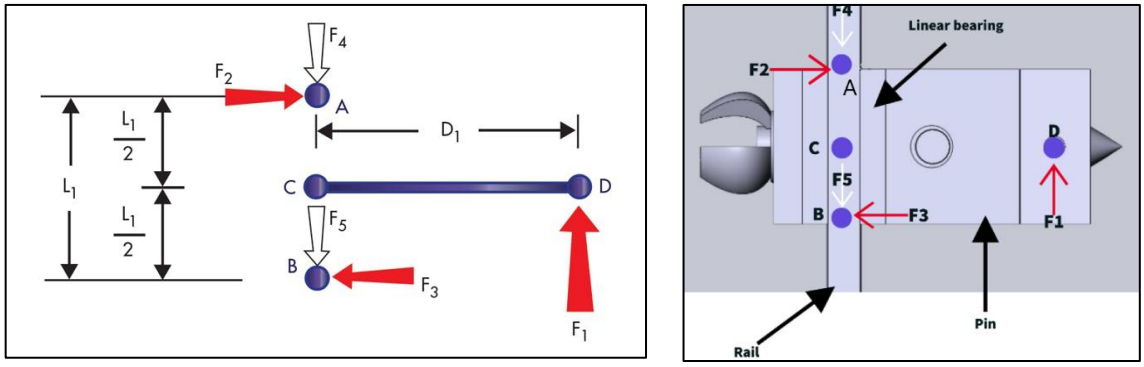

a) b)

Figure 17: **a)** Isolated forces on pin (Schroeder, 2017) **b)** Pin diagram for reference (Schroeder, 2017)

To determine the friction forces on the linear bearing another model is shown in figures 17a and 17b. Figure 17a shows a simplified diagram of the forces acting upon the linear bearing. Figure 17b matches the points and forces labelled on figure 17a to the real geometry of the pin. The timing belt attaches and exerts force at point D. C to D is the moment arm of that force relative to point C. Points A and B are the top and bottom of the linear bearing, these are the locations at which the normal forces to oppose the moment generated by the timing belt are assumed to act. This is a reasonable assumption because there is a non-zero gap between the linear bearing and the rail, the (very small) angle made between the linear bearing and the rail will cause the top and bottom of the bearing to touch the rail first, since they are the furthest distance from the bearing centre C and will move the most distance horizontally from a change in angle.

Balancing the vertical forces in this model:

$$F_1 = F_4 + F_5 \geq \mu(F_2 + F_3) = F \tag{4}$$

The linear bearing is constrained in rotation along the axis perpendicular to the page thus equating moments to zero gives:

$$L_1(F_2 + F_3) = 2F_1D_1 \tag{5}$$

Taking the friction force as $F = \frac{2\mu F_1 D_1}{L_1}$, (combining Equation 5 and the RHS of equation 4) and substituting that back into equation 2:

$$Ma = T - F = T - \frac{2\mu T D_1}{L_1} = T\left(1 - \frac{2\mu D_1}{L_1}\right)$$

$$\frac{Ma}{1-\frac{2\mu D_1}{L_1}} = T$$

Equating this to equation 3:

$$\frac{Ma}{1-\frac{2\mu D_1}{L_1}} = \frac{P}{r} - \frac{Ia}{r^2}$$

Finishing with

$$a = \frac{\frac{P}{r}}{\frac{M}{1-\frac{2\mu D_1}{L_1}} + \frac{I}{r^2}}$$

A3D. Error analysis of the acceleration test

Error analysis was carried out for the acceleration test 2 and is presented below.

$$Resolution\ of\ the\ camera\ (seconds/frame) = \frac{1}{framerate} = \frac{1}{30} = 0.033$$

$$Average\ time\ to\ completion\ for\ each\ trial\ of\ each\ run = \Sigma \frac{frames\ to\ completion\ for\ runs}{total\ runs} * Resolution$$

$$Error\ in\ frames = \pm 1\ frame$$

$$Error\ in\ time\ completion\ = MAX\ OF\ \frac{error\ in\ frame}{framerate} = \pm 0.33\ seconds\ AND\ \pm(\max run\ time - average\ run\ time)$$

$$Therefore\ error\ in\ time\ completion\ for\ all\ average\ completion\ times\ of\ all\ runs = \pm 0.33\ seconds$$

$$Error\ for\ time\ between\ stages = \frac{Error\ in\ time\ for\ completion}{number\ of\ stages}$$

$$Error\ for\ time\ between\ stages\ of\ run\ 1 = \frac{\pm 0.0333}{1} = \pm 0.0333$$

$$Error\ for\ time\ between\ stages\ of\ run\ 2 = \frac{\pm 0.0333}{1} = \pm 0.0333$$

$$Error\ for\ time\ between\ stages\ of\ run\ 3 = \frac{\pm 0.0333}{2} = \pm 0.0167$$

$$Error\ for\ time\ between\ stages\ of\ run\ 4 = \frac{\pm 0.0333}{2} = \pm 0.0167$$

$$Error\ for\ time\ between\ stages\ of\ run\ 5 = \frac{\pm 0.0333}{4} = \pm 0.0083$$

$$Error\ for\ time\ between\ stages\ of\ run\ 6 = \frac{\pm 0.0333}{8} = \pm 0.0042$$

$$Error\ for\ time\ between\ stages\ of\ run\ 7 = \frac{\pm 0.0333}{12} = \pm 0.0028$$

$$Error\ for\ the\ average\ time\ between\ stages = \frac{\Sigma(Error\ for\ time\ between\ stages)}{number\ of\ runs} = \frac{0.0333 + 0.0333 + 0.0167 + 0.0167 + 0.0083 + 0.0042 + 0.0028}{7} = \pm 0.016$$

$$Resolution\ of\ the\ camera\ (seconds/frame) = \frac{1}{framerate} = \frac{1}{30} = 0.033$$

$$Average\ time\ to\ completion\ for\ each\ trial\ of\ each\ run = \Sigma \frac{frames\ to\ completion\ for\ runs}{total\ runs} * Resolution$$

$$Error\ in\ frames = \pm 1\ frame$$

$$Error\ in\ time\ completion\ = MAX\ OF\ \frac{error\ in\ frame}{framerate} = \pm 0.33\ seconds\ AND\ \pm(\max run\ time - average\ run\ time)$$

A4. Product Design Specification Device Requirements Summary Nomenclature (Anisi, Jammot, Hayward, Langton, & Sorour, 2023)

PDS	Design Aspect	Description
1	PURPOSE	Device must consist of a component which can be manually or automatically actuated to avoid moving obstacles
2	DIMENSIONS	250x550x320mm Product must be able to fit in a third of the suitcase defined. (Folding or extending can be used.). Additional space may be requested at the expense of other devices.
3	TOTAL MASS	Mass of device 6.63kg, Product must be able to fit in a third of the suitcase defined. (Folding or extending can be used.). Additional space may be requested at the expense of other devices.
4	TARGET CONSUMER	Must be designed with children in mind. Needs to be safe, effective, and useful in introducing the field of engineering to primary school children.
5	ERGONOMICS/CONTROL	Aim of super project is to get as many underrepresented groups interested in engineering and this will include disabled students. Device must be as accessible as possible and allow for alternative input peripherals to be used.
6	AESTHETICS	Product must be appealing children (see specification point 4).
7	ENVIRONMENT OF INTENDED USE	Device is intended to be used during classroom Science, Technology, Engineering, Maths (STEM) outreach sessions which will take place in a classroom settings. This may be extended to covered outdoor stalls at events such as science fairs
8	SOUND ACTUATION	Inclusivity of components that emit sound to facilitate feedback cues
9	SAFETY	The affinity for the device to cause injury
10	ENGAGEMENT NUMBERS	The number of users which can benefit from the device simultaneously whilst in operation, should be maximised
	Design Aspect	**Description**
11	BATTERY LIFE/POWER	Device power source method and expected time between charges (>3hrs)
12	SETUP TIME	The time taken at the beginning of the session to manually set up the device and ensure all systems are working as intended (<15mins)
13	BUDGET	£1200
14	STOWED FORM FACTOR	Device must be self-contained and easy to transport in luggage and not be damaged by surrounding items.
15	OBSTACLE AVOIDING PIN	Pin structure must be back drivable to avoid damage during collisions
16	OBSTACLES	Obstacles must be secure for safety and collision purposes
17	BELT EXTENSION MECHANISM	Components must be fully enclosed and designed to ensure trapping fingers is not possible. Must tension belt sufficiently to allow a tensioner to maintain tautness. Must be able to lock in an expended position.
18	AUTOMATION/MACHINE VISION	Algorithm must be able to detect oncoming obstacles and calculate actuation speed and direction to ensure obstacle is avoided.
19	CONTROL BOARD	Must have adequate resources to store control algorithm and sensory data.